JCB Journal of Cell Biology

REPORT

Twinfilin bypasses assembly conditions and actin filament aging to drive barbed end depolymerization

Shashank Shekhar[1,2*], Gregory J. Hoeprich[1*], Jeff Gelles[2], and Bruce L. Goode[1]

Cellular actin networks grow by ATP-actin addition at filament barbed ends and have long been presumed to depolymerize at their pointed ends, primarily after filaments undergo "aging" (ATP hydrolysis and P_i release). The cytosol contains high levels of actin monomers, which favors assembly over disassembly, and barbed ends are enriched in ADP-P_i actin. For these reasons, the potential for a barbed end depolymerization mechanism in cells has received little attention. Here, using microfluidics-assisted TIRF microscopy, we show that mouse twinfilin, a member of the ADF-homology family, induces depolymerization of ADP-P_i barbed ends even under assembly-promoting conditions. Indeed, we observe in single reactions containing micromolar concentrations of actin monomers the simultaneous rapid elongation of formin-bound barbed ends and twinfilin-induced depolymerization of free barbed ends. The data show that twinfilin catalyzes dissociation of subunits from ADP-P_i barbed ends and thereby bypasses filament aging prerequisites to disassemble newly polymerized actin filaments.

Introduction

Rapid remodeling and turnover of the actin cytoskeleton is essential for many cellular processes, including cell migration, endocytosis, cytokinesis, and wound healing (Pollard and Borisy, 2003). Actin networks are assembled by nucleation and elongation factors, which seed the polymerization of new filaments and facilitate addition of ATP-actin subunits at filament barbed ends (Pollard and Borisy, 2003; Shekhar et al., 2016). Newly added subunits immediately hydrolyze ATP, producing ADP-P_i F-actin, and then release P_i at a much slower rate (0.005 s^{-1}), producing ADP F-actin (Carlier, 1987; Carlier and Pantaloni, 1986). ADP-P_i and ADP F-actin have distinct conformations, dynamics, and binding partners (Chou and Pollard, 2019; Merino et al., 2018). Notably, cofilin and its cofactors selectively target ADP ("aged") F-actin and catalyze severing and pointed end depolymerization (Carlier et al., 1997; Maciver et al., 1991). Thus, the nucleotide state of F-actin can serve as an internal "timer" for turnover of actin networks, directing disassembly to older regions of F-actin. However, some cellular actin networks, such as those at the leading edge, and sites of endocytosis turn over at a rate much faster than the actin aging process (Kaksonen et al., 2003; Lacy et al., 2019; Watanabe and Mitchison, 2002). These observations suggest that our understanding of actin disassembly mechanisms remains incomplete and that there may be cellular factors that target ADP-P_i F-actin to drive barbed end depolymerization and/or accelerate filament aging.

For two reasons, barbed end depolymerization as a potential mechanism for promoting actin disassembly in vivo has received little attention. First, barbed ends are enriched in ADP-P_i actin, which is more stable than ADP actin and does not attract cofilin. Second, the cytosol contains micromolar levels of assembly-competent ATP-actin monomers, well above the critical concentration for assembly at barbed ends (Carlier and Shekhar, 2017; Skruber et al., 2018). Therefore, under cellular conditions, free barbed ends should grow rather than depolymerize, unless there are specialized barbed end–associated factors that can promote the net depolymerization of ADP-P_i and/or ADP barbed ends even in the presence of ATP-actin monomers. Until now, such factors have not been reported.

Two evolutionarily conserved members of the ADF-homology (ADF-H) family, cofilin and twinfilin, promote actin depolymerization in vitro. Cofilin binds cooperatively to the sides of ADP-actin filaments and induces severing to promote disassembly (reviewed in Hild et al., 2014). In the absence of actin monomers, cofilin alone also modestly increases the rate of depolymerization at pointed ends, to ∼2–3 subunits s^{-1} (Shekhar and Carlier, 2017; Wioland et al., 2017) and, together with cyclase-associated protein (Srv2/CAP), increases the rate of pointed end depolymerization by >300-fold, to >50 subunits s^{-1} (Kotila et al., 2019; Shekhar et al., 2019). In contrast to cofilin, twinfilin binds poorly to the sides of actin filaments but readily

[1]Department of Biology, Brandeis University, Waltham, MA; [2]Department of Biochemistry, Brandeis University, Waltham, MA.

*S. Shekhar and G.J. Hoeprich contributed equally to this paper; Correspondence to Shashank Shekhar: shekhar@emory.edu; Bruce L. Goode: goode@brandeis.edu; S. Shekhar's present address is Departments of Physics and Cell Biology, Emory University, Atlanta, GA.

associates with barbed ends (Helfer et al., 2006; Hilton et al., 2018; Johnston et al., 2015; Paavilainen et al., 2007). Indeed, twinfilin localizes to and functions in vivo at sites of dynamic actin assembly enriched in barbed ends, including the tips of filopodia and stereocilia, lamellipodial networks, and yeast cortical actin patches (Hakala et al., 2019 *Preprint*; Johnston et al., 2015; Rzadzinska et al., 2009). A number of different in vitro activities have been reported for twinfilin, including filament capping, depolymerization, and monomer sequestration (Goode et al., 1998; Helfer et al., 2006; Hilton et al., 2018; Johnston et al., 2015; Paavilainen et al., 2007; Vartiainen et al., 2002). Clarification of twinfilin's effects on actin filament dynamics represents a crucial step in understanding its biological functions. Here, we attempted to resolve this open question using newly developed microfluidics-assisted total internal reflection fluorescence (mf-TIRF) microscopy.

Results and discussion

Two previous studies from our laboratory, both using conventional total internal reflection fluorescence (TIRF) microscopy, reported that budding yeast and mouse twinfilins accelerate barbed end depolymerization in the absence of actin monomers (Hilton et al., 2018; Johnston et al., 2015). However, a recent study using mf-TIRF microscopy reported that twinfilin slows rather than accelerates barbed end depolymerization (Hakala et al., 2019 *Preprint*). This discrepancy inspired us to carefully reexamine twinfilin's effects at barbed ends, comparing them side by side in conventional and mf-TIRF assays. Further, we compared twinfilin's effects on actin filaments in two different nucleotide states (ADP and ADP-P_i) given that in our previous studies we had not aged the filaments to the same extent as in a previous study (Hakala et al., 2019 *Preprint*).

We first examined the effects of mouse twinfilin 1 (mTwf1) on aged (ADP) F-actin barbed ends in a conventional TIRF experiment (Fig. 1 a, left) using fluorescently labeled filaments anchored to streptavidin-functionalized glass coverslips. After polymerization, filaments were incubated in TIRF buffer for 15 min to allow complete conversion to ADP F-actin. These filaments were then exposed to TIRF buffer with or without 5 µM mTwf1 (in the absence of G-actin). In the presence of 5 µM mTwf1, barbed ends depolymerized at a rate of 5.6 ± 1.5 subunits s^{-1} (± SD; Fig. 1, b and c), slightly slower than in control reactions lacking mTwf1 (7.9 ± 2.0 subunits s^{-1}). These effects are consistent with mTwf1 binding to barbed ends and slowing the dissociation of ADP-actin subunits.

We next performed mf-TIRF assays in which the filaments were only anchored at their pointed ends (Fig. 1 a, right). These assays alleviate concerns that anchoring filaments along their lengths might affect depolymerization rates. They also provide a more accurate measurement of change in filament length over time and more precise control when flowing in ingredients (Jégou et al., 2011; Shekhar, 2017). After polymerization, filaments were aged for 15 min as above. In the presence of 5 µM mTwf1, ADP barbed ends depolymerized at 3.6 ± 0.8 subunits s^{-1} (Fig. 1, c–f), whereas in control reactions lacking mTwf1, they depolymerized at 9.9 ± 1.3 subunits s^{-1}. Thus, mTwf1 exhibited the same or perhaps even stronger inhibition of depolymerization at ADP barbed ends in mf-TIRF compared with that in conventional TIRF assays. These results demonstrate that the above-mentioned discrepancy in twinfilin effects at barbed ends does not stem from differences in TIRF methods.

The recent study from Hakala et al., (2019 *Preprint*) investigated the effects of twinfilin on extensively aged ADP-actin filaments, and we noticed that in our earlier studies we had not aged filaments for as long, suggesting they may have consisted of a mixture of ADP-P_i and ADP subunits. This prompted us to directly investigate how the nucleotide state of the filaments influences twinfilin's effects at the barbed end. To keep filaments in the ADP-P_i state, they were maintained in buffer supplemented with 50 mM P_i (Fig. 2 a; Carlier and Pantaloni, 1988). In the presence of 5 µM mTwf1, ADP-P_i barbed ends depolymerized at 2.2 ± 0.3 subunits s^{-1}, approximately sevenfold faster than ADP-P_i barbed ends in control reactions lacking mTwf1 (0.3 ± 0.1 subunits s^{-1}; Fig. 2, b–d). Similar effects were observed in conventional TIRF assays (Fig. 2 d). Further, mTwf1 accelerated the rate of barbed end depolymerization for ADP-actin filaments incubated with BeF_3 (without 50 mM P_i), which essentially mimics the ADP-P_i state (Combeau and Carlier, 1988, 1989; Fig. 2 e). Thus, the ability of mTwf1 to increase the rate of barbed end depolymerization is not the result of high free P_i levels in solution, but rather the nucleotide state (ADP-P_i) of the filaments.

Taken together, these observations reveal that mTwf1 has strikingly opposite effects at barbed ends depending on their nucleotide state, accelerating depolymerization at ADP-P_i ends and slowing depolymerization at ADP ends (Fig. 2 f). Interestingly, in the absence of additional cellular factors, free ADP barbed ends depolymerize almost 33-fold faster than free ADP-P_i barbed ends (0.3 subunits s^{-1} vs. 9.9 subunits s^{-1}). In contrast, the depolymerization rates for ADP-P_i and ADP barbed ends are quite similar in the presence of mTwf1 (2.2 subunits s^{-1} and 3.6 subunits s^{-1}, respectively). Therefore, in the presence of mTwf1, new and old regions of F-actin will depolymerize at approximately the same rate. This is an effect that may be used to control the disassembly of cellular actin structures where twinfilin is known to reside (e.g., filopodia tips, stereocilia tips, and lamellipodia; Hakala et al., 2019 *Preprint*; Peng et al., 2009; Rzadzinska et al., 2009).

Our data also show that mTwf1's effects on ADP-P_i barbed end depolymerization are saturable (Fig. 2 g). The concentration dependence is consistent with a simple mechanism in which mTwf1 molecules bind independently to a site at the filament barbed end, and the maximum disassembly rate is reached when that site is fully occupied. The estimated cytosolic concentrations of twinfilin in mammalian cells and *Saccharomyces cerevisiae* are 0.5 and 1 µM, respectively (Johnston et al., 2015, 2018). Our in vitro experiments predict that these concentrations of twinfilin could strongly accelerate depolymerization.

We next considered whether mTwf1's depolymerization effects at ADP-P_i barbed ends can occur under actin assembly-promoting conditions (i.e., ATP-actin monomer levels above the barbed end critical concentration). In cells, the cytosol contains micromolar levels of assembly-competent actin monomers

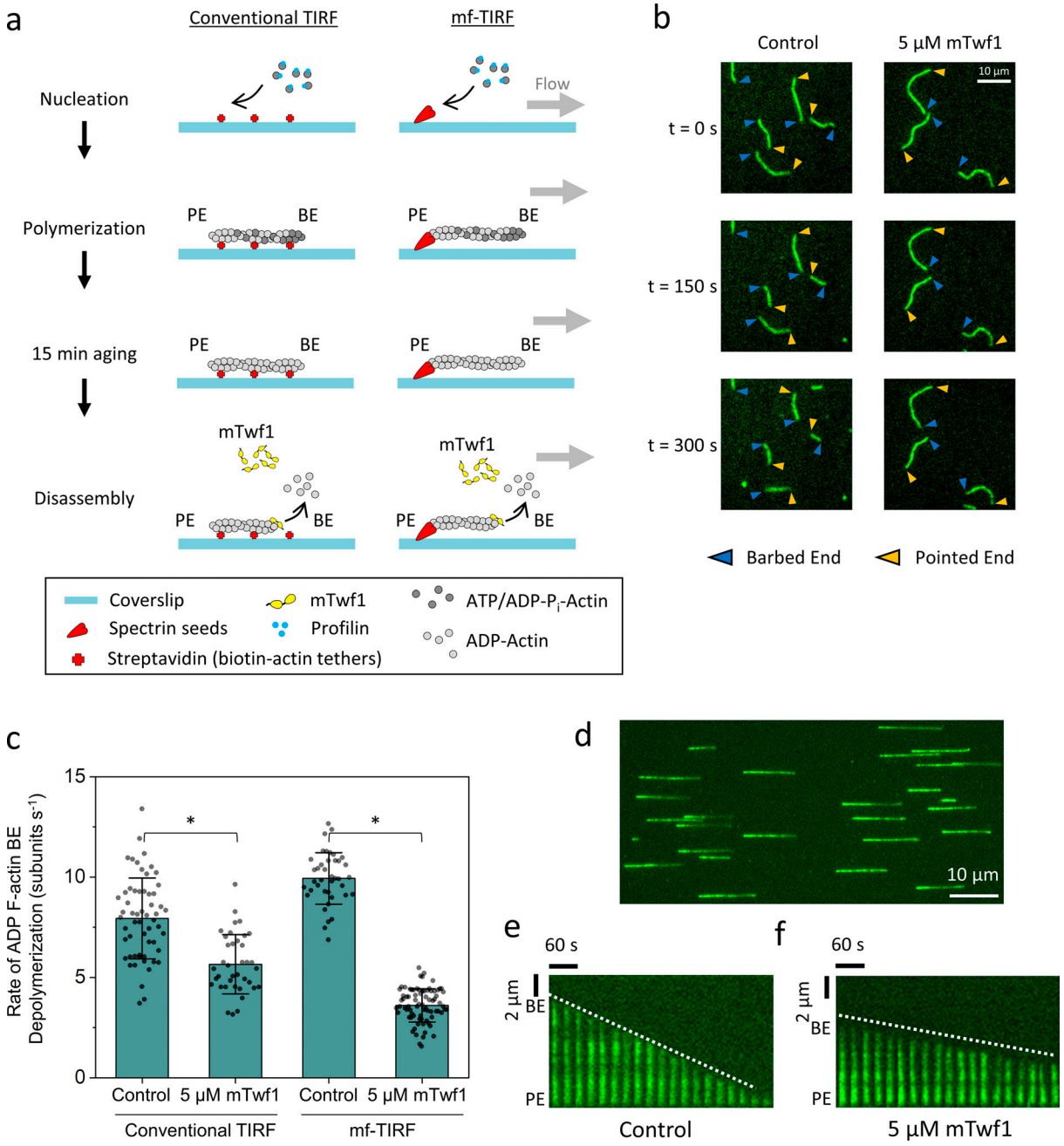

Figure 1. **mTwf1 slows the depolymerization of aged (ADP) actin filament barbed ends. (a)** Schematics of conventional TIRF and mf-TIRF experiments to monitor barbed end depolymerization of ADP-actin filaments. In conventional TIRF (left), filaments are polymerized using 2 µM G-actin (15% Alexa-488 labeled and 0.5% biotinylated) and 3 µM profilin. In mf-TIRF assays (right), filaments with free barbed ends are polymerized by exposing coverslip-anchored spectrin-actin seeds to 2 µM G-actin (15% Alexa-488 labeled) and 5 µM profilin. In both setups, filaments are aged to produce ADP F-actin by incubation for 15 min in TIRF buffer or mf-TIRF buffer containing 0.1 µM G-actin (critical concentration at the barbed end, to prevent change in filament length). Then 5 µM mTwf1 or control buffer is flowed in, and barbed end depolymerization is monitored over time. Note that G-actin and profilin are no longer present when depolymerization is monitored. BE, barbed end; PE, pointed end. **(b)** Representative time-lapse images from conventional TIRF assays showing the effects of 5 µM mTwf1 on barbed end depolymerization. Blue arrowheads, barbed ends. Yellow arrowheads, pointed ends. **(c)** Comparison of single filament rates (mean ± SD) for barbed end depolymerization in the presence and absence of 5 µM mTwf1 and in conventional TIRF and mf-TIRF assays. *, Statistical comparison by two-sample *t* test between indicated conditions ($P < 0.05$). Number of filament ends analyzed for each condition (left to right): 58, 38, 40, and 78. Conventional TIRF experiments were performed two times and mf-TIRF experiments three times and yielded similar results. Data shown are from one experiment each. **(d)** Representative field of view from mf-TIRF assay, showing filaments aligned under flow in the microfluidic chamber with anchored pointed ends (left) and free barbed ends (right). **(e)** Representative kymograph of an Alexa-488–labeled actin filament (green) depolymerizing in control buffer from mf-TIRF assay. **(f)** Same as e but in the presence of 5 µM mTwf1. White dotted lines indicate the slope of the depolymerizing barbed ends.

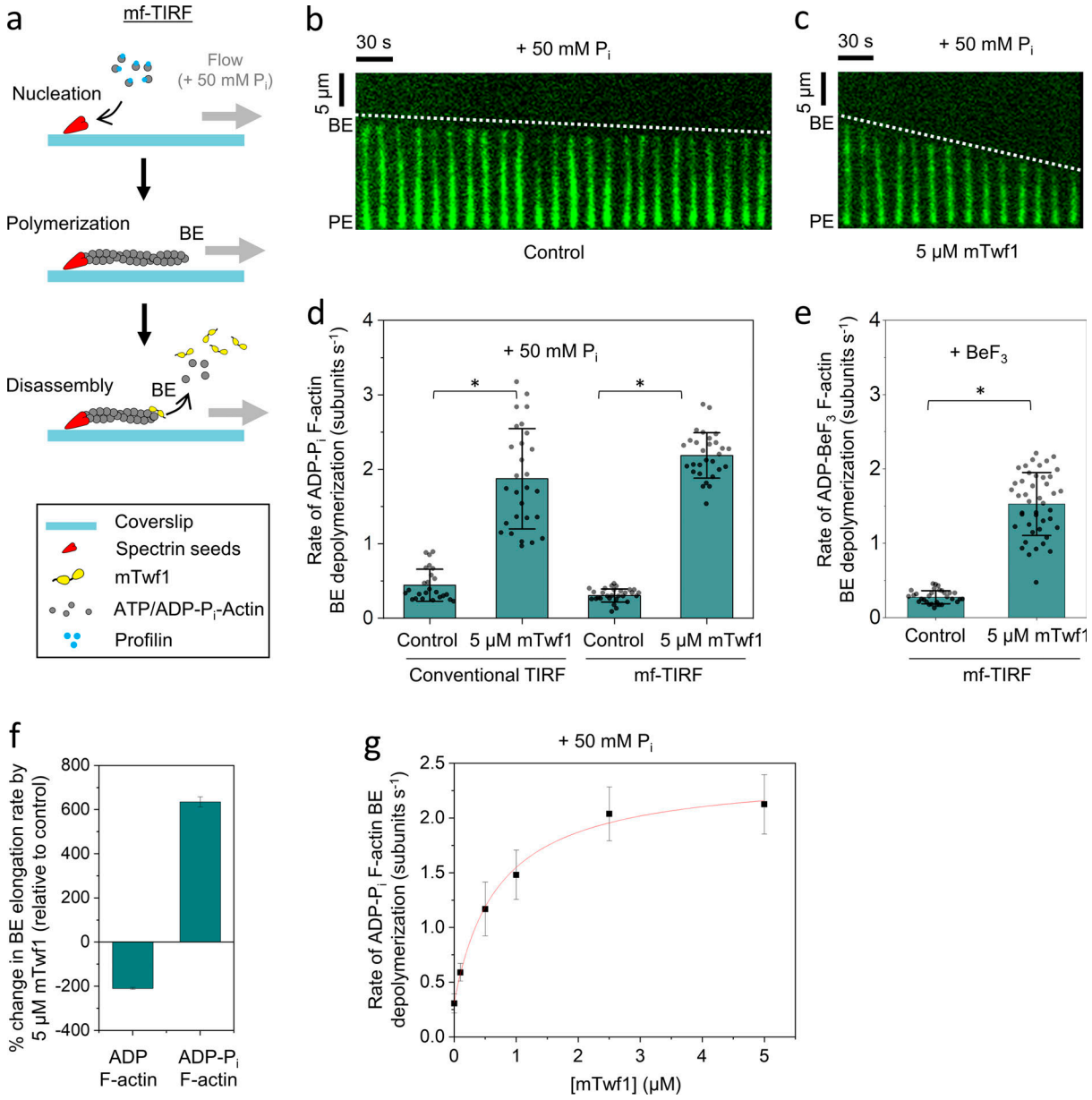

Figure 2. **mTwf1 accelerates the depolymerization of newly polymerized (ADP + P_i) actin filament barbed ends. (a)** Schematic showing the experimental strategy for measuring barbed end depolymerization of ADP-P_i actin filaments in mf-TIRF assays. Actin filaments with free barbed ends were polymerized using coverslip-anchored spectrin-actin seeds by the addition of 2 µM G-actin (15% Alexa-488 labeled) and 5 µM profilin in mf-TIRF buffer containing 50 mM P_i. Next, mf-TIRF buffer (supplemented with 50 mM P_i) with or without 5 µM mTwf1 was introduced into the chamber, and depolymerization at barbed ends was monitored. Note that G-actin and profilin were no longer present when depolymerization was monitored. BE, barbed end; PE, pointed end. **(b)** Representative kymograph of Alexa-488–labeled actin filament (green) depolymerizing in mf-TIRF buffer with 50 mM P_i (Control). **(c)** Same as b but in the presence of 5 µM mTwf1. White dotted lines indicate the slope of depolymerizing barbed ends. **(d)** Rates (mean ± SD) of barbed end depolymerization with and without 5 µM mTwf1 in conventional TIRF versus mf-TIRF assays. *, Statistical comparison by two-sample *t* test between indicated conditions ($P < 0.05$). Number of filament ends analyzed for each condition (left to right): 25, 28, 29, and 29. Note that the scale in this panel is different than that in Fig. 1 c. **(e)** Rates (mean ± SD) of barbed end depolymerization in the presence of BeF_3 with and without 5 µM mTwf1. *, Statistical comparison by two-sample *t* test between indicated conditions ($P < 0.05$). Number of filament ends analyzed for each condition (left to right): 77 and 109. **(f)** Percent change in the rate of barbed end depolymerization induced by 5 µM mTwf1 for ADP- (left) or ADP-P_i–actin (right) filaments (mean ± SEM for two replicates). **(g)** Rates (mean ± SD) of barbed end depolymerization for ADP-P_i filaments as a function of mTwf1 concentration in mf-TIRF. Number of filament ends analyzed for each concentration (left to right): 29, 45, 41, 36, 42, and 46. The line is a fit to a hyperbolic binding curve (see Materials and methods). Conventional TIRF experiments were performed two times and mf-TIRF experiments three times and yielded similar results. Data shown are from one experiment each.

(free and profilin bound), well above the ∼0.1-µM critical concentration for assembly. This favors growth over disassembly at free barbed ends, as well as at barbed ends bound to polymerization factors such as formins or Ena/VASP (Bear and Gertler, 2009; Goode and Eck, 2007). A study (Hakala et al., 2019 *Preprint*) recently called into question twinfilin's ability to drive barbed end depolymerization in the presence of G-actin and instead proposed that twinfilin sequesters actin monomers and thereby lowers the concentration of assembly-competent G-actin to indirectly cause net depolymerization under actin assembly–promoting conditions.

To clarify how twinfilin promotes barbed end depolymerization, we prepared a mixed population of filaments, some with free and some with formin (mDia1)-capped barbed ends (Fig. 3, a–c). Approximately 20% of barbed ends were capped by mDia1, as judged by their faster growth rates upon exposure to G-actin and profilin (Video 1 and Video 2). When this mixed filament population was then exposed to mTwf1 (25 nM to 5 µM) in the presence of G-actin and profilin, the formin-bound barbed ends continued to grow rapidly, at rates similar to those observed before the addition of mTwf1 (Fig. 3 d). Thus, mTwf1 does not significantly reduce the concentration of assembly-competent actin monomers under these conditions. In contrast, mTwf1 changed the dynamics of free barbed ends, slowing net polymerization at lower concentrations of mTwf1 and inducing net depolymerization at higher concentrations of mTwf1 (Fig. 3 e). We note that the rate of barbed end depolymerization observed here is higher than in Fig. 1 c. This is likely due to these reactions containing free profilin, which was included to enable formins to polymerize the barbed ends. Profilin alone increases the rate of depolymerization at barbed ends (Pernier et al., 2016). Thus, the higher rates of depolymerization we observed in these experiments could be due to the combined effects of mTwf1 and profilin on barbed end depolymerization. Importantly, our observation that free barbed ends rapidly shortened while formin-bound barbed ends continued to rapidly grow, all within the same reactions (Fig. 3, c and f; and Video 1), demonstrates that mTwf1 promotes net depolymerization of barbed ends under assembly-promoting conditions (0.5 µM G-actin) and that these effects are not due to actin monomer sequestration by mTwf1. At higher concentrations of G-actin (3 µM and 10 µM), mTwf1 continued to suppress growth and promote net depolymerization of filaments but at slower rates (Fig. 3 g). Overall, these observations show that under assembly-promoting conditions, mTwf1 attenuates growth and promotes barbed end depolymerization.

Combining the new observations here with previous work, we present a working model for twinfilin's overall regulatory effects at barbed ends (Fig. 4). Twinfilin first binds, alone or together with its interaction partner capping protein (Johnston et al., 2018; Palmgren et al., 2001), to newly polymerized (ADP-P_i) barbed ends. When capping protein alone or twinfilin and capping protein together are bound to a barbed end, filament growth is paused. Twinfilin catalyzes capping protein dissociation from barbed ends (Hakala et al., 2019 *Preprint*), leaving twinfilin alone at the barbed end to processively depolymerize ADP-P_i actin filaments (accelerating subunit dissociation while blocking the addition of new subunits).

To date, no other cellular factors have been shown to promote the net depolymerization of ADP-P_i barbed ends in the presence of excess G-actin (as found in the cytosol). Cofilin is capable of increasing the rate of dissociation of actin subunits from ADP-P_i (and ADP) barbed ends, but not in presence of actin monomers (Shekhar and Carlier, 2017; Wioland et al., 2017). We speculate that the unique ability of twinfilin to drive barbed end depolymerization under assembly-promoting conditions may arise from an ability to suppress ATP-actin subunit exchange at barbed ends while permitting the exchange of ADP-$P_{i\text{-actin}}$ and ADP-actin subunits. Further, these novel capabilities of twinfilin may stem from its specific molecular architecture, consisting of two connected ADF-H domains and a short C-terminal tail, with each domain binding to actin and contributing to its in vitro and in vivo functions (Johnston et al., 2015; Palmgren et al., 2001).

Finally, our observations reinforce the view that different ADF-H domain proteins have evolved to perform distinct roles in promoting cellular actin turnover (Hild et al., 2014). Under assembly-promoting conditions, twinfilin promotes capping protein dissociation from barbed ends and drives depolymerization of ADP-P_i F-actin, while cofilin works with AIP1 and Srv2/CAP to induce severing and accelerated pointed end depolymerization of ADP F-actin (Fig. 4; Andrianantoandro and Pollard, 2006; Blanchoin and Pollard, 1999; Brieher et al., 2006; Carlier et al., 1997; Jansen et al., 2014; Kotila et al., 2019; Michelot et al., 2007; Nadkarni and Brieher, 2014; Shekhar and Carlier, 2017; Shekhar et al., 2019; Wioland et al., 2017). The nucleotide-dependent effects of twinfilin at the barbed end allow it to bypass filament aging requirements (P_i release) and promote disassembly of recently polymerized F-actin. These activities may play an important role in the regulation of cellular actin structures that undergo rapid turnover (Carlier, 1987; Carlier and Pantaloni, 1986) and/or whose lengths are tightly controlled by growth and disassembly at barbed ends (e.g., filopodia and stereocilia tips), where twinfilin has been localized (Hakala et al., 2019 *Preprint*; Peng et al., 2009; Rzadzinska et al., 2009).

Materials and methods

Purification and labeling of actin

Rabbit skeletal muscle actin was purified from acetone powder (Spudich and Watt, 1971) generated from frozen ground hind leg muscle tissue of young rabbits (Pel-Freez). Lyophilized acetone powder stored at −80°C was mechanically sheared in a coffee grinder, resuspended in G-buffer (5 mM Tris-HCl pH 7.5, 0.5 mM DTT, 0.2 mM ATP, and 0.1 mM $CaCl_2$), and then cleared by centrifugation for 20 min at 50,000 ×*g*. Supernatant was collected and further filtered with Whatman paper. Actin was polymerized by the addition of 2 mM $MgCl_2$ and 50 mM NaCl to the filtrate and overnight incubation at 4°C with slow stirring. Next morning, NaCl powder was added to a final concentration of 0.6 M, and stirring was continued for another 30 min at 4°C. F-actin was pelleted by centrifugation for 150 min at 120,000 ×*g*, and the pellet was solubilized by dounce homogenization and dialyzed against G-buffer for 48 h at 4°C. Monomeric actin was then precleared at 435,000 ×*g* and loaded onto an S200 (16/60) gel-filtration column (GE Healthcare) equilibrated in G-buffer. Fractions containing actin were stored at 4°C.

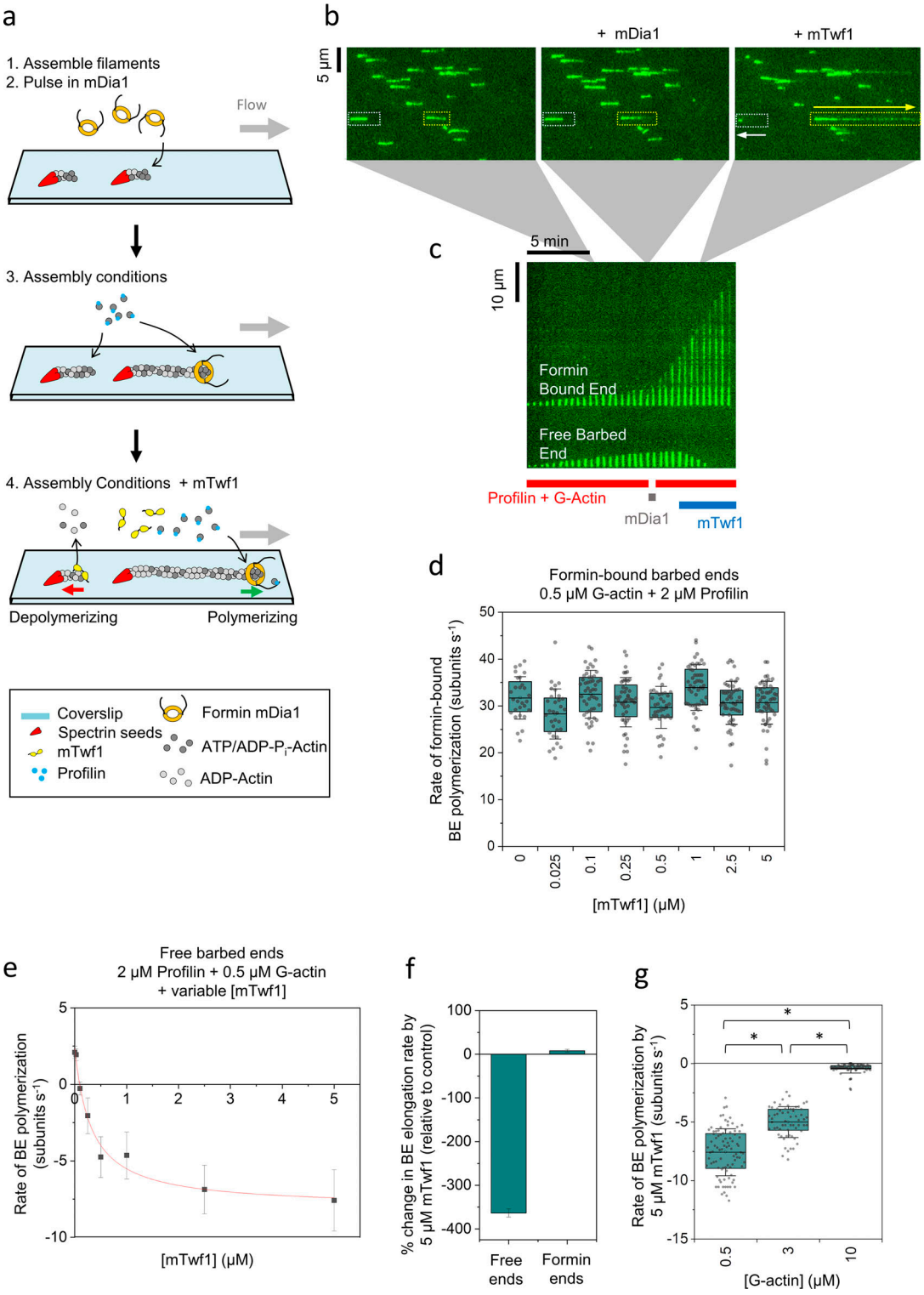

Figure 3. **mTwf1 induces depolymerization of newly polymerized barbed ends even under assembly-promoting conditions. (a)** Schematic showing the experimental strategy for investigating the effects of mTwf1 on barbed ends in assembly-promoting conditions. Filaments with free barbed ends were polymerized by exposing coverslip-anchored spectrin-actin seeds to a flow containing 0.5 µM G-actin (15% Alexa-488 labeled) and 2 µM profilin. 20 nM mDia1 was then introduced for 20 s, which resulted in ∼20% of barbed ends being capped by mDia1. The filaments were then briefly exposed to 0.5 µM G-actin (15% Alexa-488 labeled) and 2 µM profilin in mf-TIRF buffer (<1 min) to identify the fast-growing mDia1-capped ends. Next, mf-TIRF buffer containing 0.5 µM G-actin (15% Alexa-488 labeled), 2 µM profilin, and 0–5 µM mTwf1 was introduced into the chamber, and barbed end dynamics were monitored. **(b)** Representative field of view showing filaments growing at their barbed ends before mDia1 flow in (left), then the same filaments growing at their free barbed ends (white dotted rectangles) or growing more rapidly at their mDia1-capped barbed ends (yellow dotted rectangles) in the presence of actin and profilin (middle), and finally the same barbed ends shortening or elongating, respectively, after flowing in 5 µM mTwf1 with G-actin and profilin (right). White arrow denotes a

depolymerizing free barbed end, and the yellow arrow denotes a rapidly elongating formin-bound barbed end. **(c)** Kymographs of the same two filaments highlighted in b, grown in the presence of 0.5 µM G-actin and 2 µM profilin (red bar) before and after pulsing in 20 nM mDia1 (gray bar). Upon subsequent flow in of 5 µM mTwf1 with 0.5 µM G-actin and 2 µM profilin (blue bar), the free barbed end starts to depolymerize (bottom), while the mDia1-capped barbed end continues to rapidly elongate (top). **(d)** Rates (mean ± SD) of mDia1-capped barbed end elongation in the presence of 0.5 µM G-actin (15% Alexa-488 labeled), 2 µM profilin, and different concentrations of mTwf1. BE, barbed end. **(e)** Rates (mean ± SD) of free barbed end elongation in the presence of 0.5 µM G-actin, 2 µM profilin, and different concentrations of mTwf1. The red line is a fit to a hyperbolic binding curve (see Materials and methods). **(f)** Percent change in elongation rate by 5 µM mTwf1 (compared with control reactions) for free barbed ends versus mDia1-capped barbed ends (mean ± SEM for three replicates). Reactions contained 0.5 µM G-actin and 2 µM profilin, with or without 5 µM mTwf1. **(g)** Effects of 5 µM mTwf1 on rate (mean ± SD) of depolymerization of free barbed ends in the presence of different concentrations of profilin-bound actin monomers: 0.5 µM G-actin with 2 µM profilin, 3 µM G-actin with 4 µM profilin, and 10 µM G-actin with 15 µM profilin. *, Statistical comparison by two-sample *t* test between indicated conditions ($P < 0.05$). Number of filament ends analyzed for each condition (left to right): 90, 61, and 78. All experiments were performed at least three times and yielded similar results. Data shown are from one experiment each.

To biotinylate actin, the F-actin pellet above was dounced and dialyzed against G-buffer lacking DTT. Monomeric actin was then polymerized by the addition of an equal volume of 2× labeling buffer (50 mM imidazole pH 7.5, 200 mM KCl, 0.3 mM ATP, and 4 mM $MgCl_2$). After 5 min, the actin was mixed with a fivefold molar excess of NHS-XX-Biotin (Merck KGaA) and incubated in the dark for 15 h at 4°C. The F-actin was pelleted as above, and the pellet was rinsed with G-buffer, then homogenized with a dounce, and dialyzed against G-buffer for 48 h at 4°C. Biotinylated monomeric actin was purified further on an S200 (16/60) gel-filtration column as above. Aliquots of biotin-actin were snap frozen in liquid N_2 and stored at −80°C.

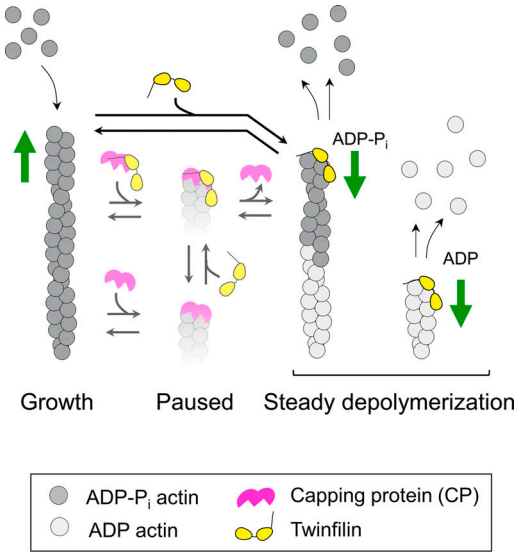

Figure 4. **Working model for twinfilin activities at actin filament barbed ends.** Actin filament barbed ends grow by the addition of ATP-actin monomers, which rapidly hydrolyze their bound ATP, producing ADP-P_i–actin subunits. Subsequently, barbed ends are bound by twinfilin alone, capping protein (CP) alone, or twinfilin-capping protein complexes, in each case inhibiting barbed end growth. Twinfilin catalyzes the dissociation of capping protein from barbed ends (Hakala et al., 2019 *Preprint*), leaving twinfilin alone at the barbed end. Twinfilin then induces the depolymerization of ADP-P_i barbed ends, even in the presence of G-actin at concentrations far above the critical concentration for assembly. We postulate that twinfilin achieves these effects using a processive barbed end tracking mechanism, which was directly observed for yeast twinfilin (Johnston et al., 2015). Once twinfilin reaches regions of ADP F-actin, its interactions with the barbed end slow the rate of depolymerization (compared with that of free ADP barbed ends).

To fluorescently label actin, G-actin was polymerized by dialyzing overnight against modified F-buffer (20 mM Pipes pH 6.9, 0.2 mM $CaCl_2$, 0.2 mM ATP, and 100 mM KCl; Shekhar, 2017). F-actin was incubated for 2 h at room temperature with a fivefold molar excess of Alexa-488 NHS ester dye (Life Technologies). The F-actin was then pelleted by centrifugation at 450,000 ×*g* for 40 min at room temperature, and the pellet was resuspended in G-buffer, homogenized with a dounce, and incubated on ice for 2 h to depolymerize the filaments. The monomeric actin was then repolymerized on ice for 1 h by the addition of 100 mM KCl and 1 mM $MgCl_2$, and the F-actin was pelleted by centrifugation for 40 min at 450,000 ×*g* at 4°C. The pellet was homogenized with a dounce and dialyzed overnight at 4°C against 1 liter of G-buffer. The solution was precleared by centrifugation at 450,000 ×*g* for 40 min at 4°C. The supernatant was collected, and the concentration and the labeling efficiency of actin were determined by measuring the absorbance at 280 nm and 495 nm, respectively. Molar extinction coefficients used were as follows: ε_{280} actin = 45,840 M^{-1} cm^{-1}, ε_{495} Alexa-488 = 71,000 M^{-1} cm^{-1}, and ε_{280} AF488 = 7,810 M^{-1} cm^{-1}.

Purification of twinfilin

mTwf1 was expressed as a GST fusion protein in *Escherichia coli* strain BL21 (pRARE). Cells were grown to log phase at 37°C, and then expression was induced for 16 h at 18°C by the addition of 0.4 mM IPTG. Cells were harvested by centrifugation, and the pellets were stored at −−80°C. Frozen cell pellets were resuspended in 10 ml of PBS supplemented freshly with 0.5 mM DTT, 1 mM PMSF, and protease inhibitors (0.5 µM each of pepstatin A, antipain, leupeptin, aprotinin, and chymostatin). Lysozyme (0.5 mg/ml) was added, and the cells were lysed by sonication using a tip sonicator while keeping the tubes on ice. The lysate was clarified by centrifugation at 12,500 ×*g* for 20 min, and then the supernatant was incubated at 4°C (rotating) for 2–3 h with 0.5 ml glutathione–agarose beads (Sigma-Aldrich). Beads were washed three times in cold PBS supplemented with 1 M NaCl and then washed twice in cold PBS.

mTwf1 was released from the beads by incubation with PreScission Protease (GE Healthcare) overnight at 4°C (rotating), thus leaving GST on the beads. The released mTwf1 was concentrated to 0.3 ml, then loaded on a Superose12 size-exclusion column (GE Healthcare) equilibrated in 20 mM Hepes pH 7.5, 1 mM EDTA, 50 mM KCl, and 0.5 mM DTT. Peak fractions were pooled, concentrated, aliquoted, snap frozen in liquid N_2, and stored at −80°C.

Purification of profilin

Human profilin-1 was expressed in *E. coli* BL21 DE3 by growing cells to log phase at 37°C in Terrific Broth (TB) medium and inducing expression with 1 mM IPTG at 37°C for 3 h. Cells were harvested by centrifugation, and pellets were stored at −80°C. Cell pellets were resuspended in lysis buffer (50 mM Tris-HCl pH 8.0, 1 mM EDTA, 0.2% Triton X-100, and lysozyme + protease inhibitors as above), kept on ice for 30 min, and then further lysed by sonication. Lysates were cleared for 25 min at 272,000 ×*g* at 4°C, and the supernatant was collected and fractionated on a HiTrap Q column (buffer: 20 mM Tris-HCl, pH 8.0). Peak fractions were concentrated and then purified further on a Superdex 75 column equilibrated in 20 mM Tris-HCl pH 8.0, and 50 mM NaCl. Peak fractions were pooled, aliquoted, snap frozen in liquid N_2, and stored at −80°C.

Conventional TIRF microscopy

Glass coverslips (60 × 24 mm; Thermo Fisher Scientific) were first cleaned by sonication in detergent for 60 min, followed by successive sonications in 1 M KOH and 1 M HCl for 20 min each and in ethanol for 60 min. Coverslips were then washed extensively with H_2O and dried in an N_2 stream. The cleaned coverslips were coated with 2 mg/ml methoxy–poly(ethylene glycol [PEG])–silane MW 2,000 and 2 µg/ml biotin-PEG-silane MW 3,400 (Laysan Bio) in 80% ethanol pH 2.0, and incubated overnight at 70°C. Flow cells were assembled by rinsing PEG-coated coverslips with water, drying with N_2, and adhering to µ-Slide VI0.1 (0.1 × 17 × 1 mm) flow chambers (Ibidi) with double-sided tape (2.5 cm × 2 mm × 120 µm) and 5-min epoxy resin (Devcon). Before each reaction, the flow cell was sequentially incubated for 1 min each with 4 µg/ml streptavidin in HEK buffer (20 mM Hepes pH 7.4, 1 mM EDTA, 50 mM KCl, and 5% glycerol) and 1% BSA in HEK buffer. The flow cell was then equilibrated with TIRF buffer (10 mM imidazole pH 7.4, 50 mM KCl, 1 mM $MgCl_2$, 1 mM EGTA, 0.2 mM ATP, 10 mM DTT, 15 mM glucose, 20 µg/ml catalase, 100 µg/ml glucose oxidase, and 0.5% methylcellulose [4,000 cP]). Actin filaments were grown using 2 µM G-actin (15% Alexa-488 labeled and 0.5% biotinylated G-actin) and 3 µM profilin until they reached lengths of ∼10–20 µm. After this assembly phase, the filaments were aged (to produce ADP actin) by incubating them for 15 min in TIRF buffer in the presence of 0.1 µM G-actin (to prevent their depolymerization during aging). We then flowed in mTwf1 diluted in TIRF buffer or buffer alone and monitored change in filament length over time. For experiments with ADP-P_i–actin filaments, the filaments were polymerized using 2 µM ATP–G-actin and 3 µM profilin in modified TIRF buffer containing 50 mM PO_4 (the 50 mM KCl was replaced with 34.8 mM K_2HPO_4 and 15.2 mM KH_2PO_4). Effects of mTwf1 on ADP-P_i barbed ends were monitored in the continuous presence of modified TIRF buffer.

mf-TIRF microscopy

Actin filaments were first assembled in mf-TIRF flow cells (Jégou et al., 2011; Shekhar, 2017; Shekhar and Carlier, 2016, 2017). Coverslips were first cleaned by sonication in detergent for 60 min, followed by successive sonications in 1 M KOH and 1 M HCl for 20 min each and in ethanol for 60 min. Coverslips were then washed extensively with H_2O and dried in an N_2 stream. The cleaned coverslips were coated with an 80% ethanol solution adjusted to pH 2.0 with HCl containing 2 mg/ml methoxy-PEG–silane MW 2,000 and incubated overnight at 70°C. A 40-µm-high Polydimethylsiloxane (PDMS) mold with three inlets and one outlet was mechanically clamped onto a PEG-silane–coated coverslip. The chamber was then connected to a Maesflo microfluidic flow-control system (Fluigent), rinsed with mf-TIRF buffer (10 mM imidazole pH 7.4, 50 mM KCl, 1 mM $MgCl_2$, 1 mM EGTA, 0.2 mM ATP, 10 mM DTT, 15 mM glucose, 20 µg/ml catalase, and 100 µg/ml glucose oxidase) and incubated with 1% BSA and 10 µg/ml streptavidin in mf-TIRF buffer for 5 min. Spectrin-actin seeds were nonspecifically anchored on the glass coverslip. Actin filaments with free barbed ends were formed by exposing spectrin-actin seeds to a flow containing 2 µM G-actin (15% Alexa-488 labeled) and 5 µM profilin in mf-TIRF buffer at room temperature.

After filaments were polymerized in mf-TIRF flow cells, barbed-end depolymerization was monitored at room temperature as follows. For experiments on ADP-actin filaments, newly polymerized filaments were aged for 15 min under continuous flow in mf-TIRF buffer containing 0.1 µM G-actin (unlabeled) before monitoring depolymerization. For experiments on ADP-P_i actin filaments, the polymerized filaments were maintained in the presence of modified mf-TIRF buffer containing 50 mM PO_4 (where 50 mM KCl was replaced by 34.8 mM K_2HPO_4 and 15.2 mM KH_2PO_4). For experiments on ADP-BeF_3 actin filaments, the polymerized filaments were maintained in the presence of modified mf-TIRF buffer containing 5 mM NaF and 100 µM $BeSO_4$ (Combeau and Carlier, 1988, 1989).

Image acquisition and analysis

Single-wavelength time-lapse TIRF imaging was performed on a Nikon-Ti2000 inverted microscope equipped with a 150-mW Argon laser (Melles Griot), a 60× TIRF-objective with a numerical aperture of 1.49 (Nikon Instruments Inc.), and an electron-multiplying charge-coupled device (EMCCD) camera (Andor Ixon). One pixel was equivalent to 143 × 143 nm. Focus was maintained by the Perfect Focus system (Nikon Instruments Inc.). Images were acquired every 5 s or 10 s and exposed for 100 ms using imaging software Elements (Nikon Instruments Inc.).

Images were analyzed in Fiji (Schindelin et al., 2012). Drift correction was performed using coverslip-anchored streptavidin-functionalized TransFluoSpheres (Thermo Fisher Scientific) and processing of the images with the MultiStackReg plugin. Background subtraction was conducted using the rolling ball background subtraction algorithm (ball radius, 5 pixels). For conventional TIRF assays, depolymerization rates were determined by tracking the initial and final positions of the actin filament barbed ends using the MTrackJ plugin. For mf-TIRF assays, the kymograph plugin was used to draw kymographs of individual filaments. The kymograph slope was used to calculate barbed end depolymerization rate of each individual filament (assuming one actin subunit contributes 2.7 nm to filament length). Data analysis and curve fitting were performed in Microcal Origin. Depolymerization rate (*D*) data (Fig. 2 g) and

polymerization rate (P) data (Fig. 3 e) were fit to the hyperbolic binding curve:

$$D = \quad - P = D_0 + \frac{(D_{max} - D_0)\ C}{K + C},$$

where C is the mTwf1 concentration, D_0 is the rate of depolymerization in the absence of mTwf1, D_{max} is the rate of depolymerization at saturating mTwf1 concentration, and K is the mTwf1 concentration at half-saturation. Fitting the data in Fig. 2 g to this equation gives D_{max} = 2.4 ± 0.1 subunits s^{-1}, D_0 = 0.32 ± 0.02 subunits s^{-1}, and K = 0.7 ± 0.1 µM, and fitting the data in Fig. 3 e gives D_{max} = 8.0 ± 0.9 subunits s^{-1}, D_0 = 2.3 ± 0.2 subunits s^{-1}, and K = 0.3 ± 0.1 µM.

Percent changes in elongation rate in the presence of mTwf1 (Fig. 2 f and Fig. 3 f) were determined using the following equation:

$$\frac{(R_T - R_c)}{R_c} * 100,$$

where R_T and R_c are the rates of barbed end elongation in the presence of twinfilin (R_T) or control buffer (R_c).

Statistical analysis

As indicated in the legend for each figure, all experiments were repeated multiple times and yielded similar results. Data shown are from one experiment each. Means and errors (SD or SEM) were calculated using Microcal Origin. Data distributions were assumed to be normal, but this was not formally tested. Statistical comparison between indicated conditions was conducted using the two-sample t test (Fig. 1 c; Fig. 2, d and e; and Fig. 3 g). Differences were considered significant if the P value was <0.05 (*).

Data availability

Data supporting the findings of this manuscript are available from the corresponding author upon reasonable request.

Online supplemental material

Video 1 and Video 2 show that twinfilin promotes depolymerization of actin filament–free barbed ends under assembly-promoting conditions while having no effect on the rate of elongation of formin-capped barbed ends in the same reactions.

Acknowledgments

We thank Marie-France Carlier and Tom Pollard for advice on how to keep actin filaments in the ADP-P_i state and how to use BeF_3 to mimic the ADP-P_i state.

This research was supported by the Brandeis University National Science Foundation Materials Research Science and Engineering Center, grant 142038, and by grants from the National Institutes of Health to B.L. Goode (R35 GM134895) and to B.L. Goode and J. Gelles (R01 GM098143).

The authors declare no competing financial interests.

Author contributions: S. Shekhar, G.J. Hoeprich, J. Gelles, and B.L. Goode designed the experiments and wrote the manuscript. S. Shekhar and G.J. Hoeprich performed experiments and analyzed the data.

Submitted: 3 June 2020
Revised: 6 October 2020
Accepted: 29 October 2020

References

Andrianantoandro, E., and T.D. Pollard. 2006. Mechanism of actin filament turnover by severing and nucleation at different concentrations of ADF/cofilin. *Mol. Cell.* 24:13–23. https://doi.org/10.1016/j.molcel.2006.08.006

Bear, J.E., and F.B. Gertler. 2009. Ena/VASP: towards resolving a pointed controversy at the barbed end. *J. Cell Sci.* 122:1947–1953. https://doi.org/10.1242/jcs.038125

Blanchoin, L., and T.D. Pollard. 1999. Mechanism of interaction of Acanthamoeba actophorin (ADF/Cofilin) with actin filaments. *J. Biol. Chem.* 274:15538–15546. https://doi.org/10.1074/jbc.274.22.15538

Brieher, W.M., H.Y. Kueh, B.A. Ballif, and T.J. Mitchison. 2006. Rapid actin monomer-insensitive depolymerization of Listeria actin comet tails by cofilin, coronin, and Aip1. *J. Cell Biol.* 175:315–324. https://doi.org/10.1083/jcb.200603149

Carlier, M.F. 1987. Measurement of Pi dissociation from actin filaments following ATP hydrolysis using a linked enzyme assay. *Biochem. Biophys. Res. Commun.* 143:1069–1075. https://doi.org/10.1016/0006-291X(87)90361-5

Carlier, M.F., and D. Pantaloni. 1986. Direct evidence for ADP-inorganic phosphate-F-actin as the major intermediate in ATP-actin polymerization. Rate of dissociation of inorganic phosphate from actin filaments. *Biochemistry.* 25:7789–7792. https://doi.org/10.1021/bi00372a001

Carlier, M.F., and D. Pantaloni. 1988. Binding of phosphate to F-ADP-actin and role of F-ADP-Pi-actin in ATP-actin polymerization. *J. Biol. Chem.* 263:817–825.

Carlier, M.F., and S. Shekhar. 2017. Global treadmilling coordinates actin turnover and controls the size of actin networks. *Nat. Rev. Mol. Cell Biol.* 18:389–401. https://doi.org/10.1038/nrm.2016.172

Carlier, M.F., V. Laurent, J. Santolini, R. Melki, D. Didry, G.X. Xia, Y. Hong, N.H. Chua, and D. Pantaloni. 1997. Actin depolymerizing factor (ADF/cofilin) enhances the rate of filament turnover: implication in actin-based motility. *J. Cell Biol.* 136:1307–1322. https://doi.org/10.1083/jcb.136.6.1307

Chou, S.Z., and T.D. Pollard. 2019. Mechanism of actin polymerization revealed by cryo-EM structures of actin filaments with three different bound nucleotides. *Proc. Natl. Acad. Sci. USA.* 116:4265–4274. https://doi.org/10.1073/pnas.1807028115

Combeau, C., and M.F. Carlier. 1988. Probing the mechanism of ATP hydrolysis on F-actin using vanadate and the structural analogs of phosphate BeF-3 and AlF-4. *J. Biol. Chem.* 263:17429–17436.

Combeau, C., and M.F. Carlier. 1989. Characterization of the aluminum and beryllium fluoride species bound to F-actin and microtubules at the site of the gamma-phosphate of the nucleotide. *J. Biol. Chem.* 264:19017–19021.

Goode, B.L., and M.J. Eck. 2007. Mechanism and function of formins in the control of actin assembly. *Annu. Rev. Biochem.* 76:593–627. https://doi.org/10.1146/annurev.biochem.75.103004.142647

Goode, B.L., D.G. Drubin, and P. Lappalainen. 1998. Regulation of the cortical actin cytoskeleton in budding yeast by twinfilin, a ubiquitous actin monomer-sequestering protein. *J. Cell Biol.* 142:723–733. https://doi.org/10.1083/jcb.142.3.723

Hakala, M., H. Wioland, M. Tolonen, A. Jegou, G. Romet-Lemonne, and P. Lappalainen. 2019. Twinfilin uncaps filament barbed ends to promote turnover of lamellipodial actin networks. *bioRxiv.* doi:10.1101/864769 (Preprint posted December 4, 2019)

Helfer, E., E.M. Nevalainen, P. Naumanen, S. Romero, D. Didry, D. Pantaloni, P. Lappalainen, and M.F. Carlier. 2006. Mammalian twinfilin sequesters ADP-G-actin and caps filament barbed ends: implications in motility. *EMBO J.* 25:1184–1195. https://doi.org/10.1038/sj.emboj.7601019

Hild, G., L. Kalmár, R. Kardos, M. Nyitrai, and B. Bugyi. 2014. The other side of the coin: functional and structural versatility of ADF/cofilins. *Eur. J. Cell Biol.* 93:238–251. https://doi.org/10.1016/j.ejcb.2013.12.001

Hilton, D.M., R.M. Aguilar, A.B. Johnston, and B.L. Goode. 2018. Species-Specific Functions of Twinfilin in Actin Filament Depolymerization. *J. Mol. Biol.* 430:3323–3336. https://doi.org/10.1016/j.jmb.2018.06.025

Jansen, S., A. Collins, L. Golden, O. Sokolova, and B.L. Goode. 2014. Structure and mechanism of mouse cyclase-associated protein (CAP1) in regulating actin dynamics. *J. Biol. Chem.* 289:30732–30742. https://doi.org/10.1074/jbc.M114.601765

Jégou, A., T. Niedermayer, J. Orbán, D. Didry, R. Lipowsky, M.F. Carlier, and G. Romet-Lemonne. 2011. Individual actin filaments in a microfluidic flow reveal the mechanism of ATP hydrolysis and give insight into the properties of profilin. *PLoS Biol.* 9:e1001161. https://doi.org/10.1371/journal.pbio.1001161

Johnston, A.B., A. Collins, and B.L. Goode. 2015. High-speed depolymerization at actin filament ends jointly catalysed by Twinfilin and Srv2/CAP. *Nat. Cell Biol.* 17:1504–1511.

Johnston, A.B., D.M. Hilton, P. McConnell, B. Johnson, M.T. Harris, A. Simone, G.K. Amarasinghe, J.A. Cooper, and B.L. Goode. 2018. A novel mode of capping protein-regulation by twinfilin. *eLife.* 7:e41313. https://doi.org/10.7554/eLife.41313

Kaksonen, M., Y. Sun, and D.G. Drubin. 2003. A pathway for association of receptors, adaptors, and actin during endocytic internalization. *Cell.* 115:475–487. https://doi.org/10.1016/S0092-8674(03)00883-3

Kotila, T., H. Wioland, G. Enkavi, K. Kogan, I. Vattulainen, A. Jégou, G. Romet-Lemonne, and P. Lappalainen. 2019. Mechanism of synergistic actin filament pointed end depolymerization by cyclase-associated protein and cofilin. *Nat. Commun.* 10:5320. https://doi.org/10.1038/s41467-019-13213-2

Lacy, M.M., D. Baddeley, and J. Berro. 2019. Single-molecule turnover dynamics of actin and membrane coat proteins in clathrin-mediated endocytosis. *eLife.* 8:e52355. https://doi.org/10.7554/eLife.52355

Maciver, S.K., H.G. Zot, and T.D. Pollard. 1991. Characterization of actin filament severing by actophorin from Acanthamoeba castellanii. *J. Cell Biol.* 115:1611–1620. https://doi.org/10.1083/jcb.115.6.1611

Merino, F., S. Pospich, J. Funk, T. Wagner, F. Küllmer, H.D. Arndt, P. Bieling, and S. Raunser. 2018. Structural transitions of F-actin upon ATP hydrolysis at near-atomic resolution revealed by cryo-EM. *Nat. Struct. Mol. Biol.* 25:528–537. https://doi.org/10.1038/s41594-018-0074-0

Michelot, A., J. Berro, C. Guérin, R. Boujemaa-Paterski, C.J. Staiger, J.L. Martiel, and L. Blanchoin. 2007. Actin-filament stochastic dynamics mediated by ADF/cofilin. *Curr. Biol.* 17:825–833. https://doi.org/10.1016/j.cub.2007.04.037

Nadkarni, A.V., and W.M. Brieher. 2014. Aip1 destabilizes cofilin-saturated actin filaments by severing and accelerating monomer dissociation from ends. *Curr. Biol.* 24:2749–2757. https://doi.org/10.1016/j.cub.2014.09.048

Paavilainen, V.O., M. Hellman, E. Helfer, M. Bovellan, A. Annila, M.F. Carlier, P. Permi, and P. Lappalainen. 2007. Structural basis and evolutionary origin of actin filament capping by twinfilin. *Proc. Natl. Acad. Sci. USA.* 104:3113–3118. https://doi.org/10.1073/pnas.0608725104

Palmgren, S., P.J. Ojala, M.A. Wear, J.A. Cooper, and P. Lappalainen. 2001. Interactions with PIP2, ADP-actin monomers, and capping protein regulate the activity and localization of yeast twinfilin. *J. Cell Biol.* 155:251–260. https://doi.org/10.1083/jcb.200106157

Peng, A.W., I.A. Belyantseva, P.D. Hsu, T.B. Friedman, and S. Heller. 2009. Twinfilin 2 regulates actin filament lengths in cochlear stereocilia. *J. Neurosci.* 29:15083–15088. https://doi.org/10.1523/JNEUROSCI.2782-09.2009

Pernier, J., S. Shekhar, A. Jegou, B. Guichard, and M.F. Carlier. 2016. Profilin Interaction with Actin Filament Barbed End Controls Dynamic Instability, Capping, Branching, and Motility. *Dev. Cell.* 36:201–214. https://doi.org/10.1016/j.devcel.2015.12.024

Pollard, T.D., and G.G. Borisy. 2003. Cellular motility driven by assembly and disassembly of actin filaments. *Cell.* 112:453–465. https://doi.org/10.1016/S0092-8674(03)00120-X

Rzadzinska, A.K., E.M. Nevalainen, H.M. Prosser, P. Lappalainen, and K.P. Steel. 2009. MyosinVIIa interacts with Twinfilin-2 at the tips of mechanosensory stereocilia in the inner ear. *PLoS One.* 4:e7097. https://doi.org/10.1371/journal.pone.0007097

Schindelin, J., I. Arganda-Carreras, E. Frise, V. Kaynig, M. Longair, T. Pietzsch, S. Preibisch, C. Rueden, S. Saalfeld, B. Schmid, et al. 2012. Fiji: an open-source platform for biological-image analysis. *Nat. Methods.* 9:676–682. https://doi.org/10.1038/nmeth.2019

Shekhar, S. 2017. Microfluidics-Assisted TIRF Imaging to Study Single Actin Filament Dynamics. *Curr. Protoc. Cell Biol.* 77:12.13.1–12.13.24.

Shekhar, S., and M.F. Carlier. 2016. Single-filament kinetic studies provide novel insights into regulation of actin-based motility. *Mol. Biol. Cell.* 27:1–6. https://doi.org/10.1091/mbc.E15-06-0352

Shekhar, S., and M.F. Carlier. 2017. Enhanced Depolymerization of Actin Filaments by ADF/Cofilin and Monomer Funneling by Capping Protein Cooperate to Accelerate Barbed-End Growth. *Curr. Biol.* 27:1990–1998.e5.

Shekhar, S., J. Pernier, and M.F. Carlier. 2016. Regulators of actin filament barbed ends at a glance. *J. Cell Sci.* 129:1085–1091. https://doi.org/10.1242/jcs.179994

Shekhar, S., J. Chung, J. Kondev, J. Gelles, and B.L. Goode. 2019. Synergy between Cyclase-associated protein and Cofilin accelerates actin filament depolymerization by two orders of magnitude. *Nat. Commun.* 10:5319. https://doi.org/10.1038/s41467-019-13268-1

Skruber, K., T.A. Read, and E.A. Vitriol. 2018. Reconsidering an active role for G-actin in cytoskeletal regulation. *J. Cell Sci.* 131:jcs203760. https://doi.org/10.1242/jcs.203760

Spudich, J.A., and S. Watt. 1971. The regulation of rabbit skeletal muscle contraction. I. Biochemical studies of the interaction of the tropomyosin-troponin complex with actin and the proteolytic fragments of myosin. *J. Biol. Chem.* 246:4866–4871.

Vartiainen, M.K., T. Mustonen, P.K. Mattila, P.J. Ojala, I. Thesleff, J. Partanen, and P. Lappalainen. 2002. The three mouse actin-depolymerizing factor/cofilins evolved to fulfill cell-type-specific requirements for actin dynamics. *Mol. Biol. Cell.* 13:183–194. https://doi.org/10.1091/mbc.01-07-0331

Watanabe, N., and T.J. Mitchison. 2002. Single-molecule speckle analysis of actin filament turnover in lamellipodia. *Science.* 295:1083–1086. https://doi.org/10.1126/science.1067470

Wioland, H., B. Guichard, Y. Senju, S. Myram, P. Lappalainen, A. Jégou, and G. Romet-Lemonne. 2017. ADF/Cofilin Accelerates Actin Dynamics by Severing Filaments and Promoting Their Depolymerization at Both Ends. *Curr. Biol.* 27:1956–1967.e7.

JCB

Supplemental material

Video 1. **mTwf1 promotes the depolymerization of free barbed ends even under assembly-promoting conditions.** Alexa-488–labeled actin filaments (green) anchored at their pointed ends (magenta arrowheads) and growing at their free barbed ends (yellow arrowheads) were transiently exposed to 20 nM of the formin mDia1 (FH1-FH2-C). Filaments were then exposed to a continuous flow of 0.5 µM G-actin and 2 µM profilin to identify fast-growing mDia1-capped barbed ends (red arrowheads) and slow-growing free barbed ends (yellow arrowheads). Finally, filaments were exposed to a continuous flow of 0.5 µM G-actin, 2 µM profilin, and 5 µM mTwf1. Under these assembly-promoting conditions, the mDia1-capped barbed ends continued to rapidly elongate, while free barbed ends depolymerized. Playback speed is 15 frames per second.

Video 2. **Control reaction under assembly-promoting conditions showing that in the absence of mTwf1, free and formin-capped barbed ends both continue to polymerize, as expected.** Alexa-488–labeled actin filaments (green) anchored at their pointed ends (magenta arrowheads) and growing at their free barbed ends (yellow arrowheads) were transiently exposed to 20 nM of the formin mDia1 (FH1-FH2-C). Filaments were then exposed to a continuous flow of 0.5 µM G-actin and 2 µM profilin. Under these assembly-promoting conditions, free barbed ends (yellow arrowheads) and mDia1-capped barbed ends (red arrowheads) elongated. Playback speed is 25 frames per second.